mm, $\lambda_1 + \lambda_2 =$ mm, $\lambda_h = 2.4$ mm, $W_H = 0.2$ mm, $\lambda_c = 9.5$ mm, $W_c = 5$ mm, and $g = 0.4$ mm. Figure 4 depicts the simulated results of the conventional three-stage PC-BPF and the proposed filters with $\lambda_2 = 0$ to 3 mm. It exhibits that for the proposed filter the growing second harmonic was significantly suppressed and the rejection bandwidth was extended by increasing the value λ_2. As the measured results in Figure 5, for interlaced length $\lambda_2 = 0$ mm the second harmonic suppression was from −19 to −53 dB when compared with the conventional PC-BPF. Moreover, its insertion loss and return loss at center frequency are −1.5 and −19 dB, respectively. In addition, the −20 dB rejection bandwidth was even achieved 4.5 GHz with the interlaced length $\lambda_2 = 3$ mm that stands for 40% improvement.

4. CONCLUSION

A wide rejection bandwidth bandpass filter with SIH resonator and interlaced coupled-line has been proposed in this paper. This filter was described significantly; it improves the performance of conventional parallel couple-line structure. The interlaced couple-line can extend the rejection bandwidth for 40% improvement, and the SIH resonator can not only suppress the $2f_O$ spurious but also steepen the upper roll off characteristic. Furthermore, its insertion loss and return loss can be maintained at an acceptable level. With implementation and measurement, it is verified for our design concept.

REFERENCES

1. D.M. Pozar, Microwave engineering, 2nd ed., Wiley, New York, 1998, Ch. 8.
2. J.T. Kuo and E. Shih, Microstrip stepped impedance resonator bandpass filter with an extended optimal rejection bandwidth, IEEE Trans Microwave Theory Tech, 51 (2003), 1554–1559.
3. T. Lopetegi, M.A.G. Laso, J.H.M. Bacaicoa, D. Benito, M.J. Garde, M. Sorolla, and M. Guglielmi, New microstrip "Wiggly-Line " filters with spurious passband suppression, IEEE Trans Microwave Theory Tech, 49 (2001), 1593–1598
4. C. Quendo, E. Rius, C. Person, and M. Ney, Integration of optimized low-pass filters in a bandpass filter for out-of-band improvement, Microwave Theory Tech IEEE Trans 49 (2001), 2376–2383, 2001.
5. M.C. Velazquez-Ahumada, J. Martel, and F. Medina, Parallel coupled microstrip filters with ground-plane aperture for spurious band suppression and enhanced coupling, IEEE Trans Microwave Theory Tech, 52 (2004), 1082–1086.
6. L.-H. Hsieh and K. Chang, Compact elliptic-function low-pass filters using microstrip stepped-impedance hairpin resonators, Microwave Theory Tech IEEE Trans, 51 (Part 1) (2003), 193–199.
7. S.Y. Lee and C.M. Tsai, New cross-coupled filter design using improved hairpin resonator, IEEE Tran Microwave Theory Tech, 48 (2000), 2842–2490.

OPTIMAL SYMPLECTIC INTEGRATORS FOR NUMERICAL SOLUTION OF TIME-DOMAIN MAXWELL'S EQUATIONS

Z. X. Huang, X. L. Wu, W. Sha, and M. S. Chen
Key Laboratory of Intelligent Computing and Signal Processing
Ministry of Education, Anhui University, Hefei 230039, China

Received 24 July 2006

ABSTRACT: *Optimal symplectic integrators were proposed to improve the accuracy in numerical solution of time-domain Maxwell's equations. The proposed symplectic scheme has almost the same stability and numerical dispersion as the mostly used fourth-order symplectic scheme, but acquires more efficiency in the calculations at the same computational cost.* Microwave Opt Technol Lett 49: 545–547, 2007; Published online in Wiley InterScience (www.interscience.wiley.com). DOI 10.1002/mop.22193

Key words: *symplectic integrators; stability; numerical dispersion*

1. INTRODUCTION

Symplectic integrator schemes show substantial benefits in the fields of physics ranging from classical mechanics, electromagnetism, and quantum mechanics [1–3]. In this article, we obtained the optimal symplectic integrators based on the similar approach as presented in Ref. 4.

First, consider the following general system of ordinary differential equations

$$\frac{du}{dt} = (A + B)u, \quad 0 \le t < +\infty \tag{1}$$

We can write the mapping from $t = 0$ to $t = \Delta t$, as evolution equations of the form

$$u(t) = \exp[\Delta t(A + B)]u(0) \tag{2}$$

where A and B are noncommuting operators, which can be solved by approximating exp $[\Delta t\ (A + B)]$ to the nth-order in the product form

$$\exp[\Delta t(A + B)] = \prod_{p=1}^{m} \exp(\Delta t D_p B)\exp(\Delta t C_p A) + O((\Delta t)^{n+1}) \tag{3}$$

via a well chosen set of factorization or decomposition coefficients $\{C_p\}$and $\{D_p\}$, m and n ($m \ge n$) are the number of stages and the order of scheme, respectively. Generally, Eq. (1) results in a class of factorized symplectic integrators scheme. To determine the coefficients C_p and D_p, we expand the left hand side and right hand side of Eq. (3) in powers of Δt. The coefficients C_p and D_p of the nth-order scheme are determined, when we want the two expressions to agree up to $(\Delta t)^n$. In this article, we will consider only the symmetric factorization scheme such that $C_p = C_{m+1-p}$ $(0 < p < m + 1)$, $D_p = D_{m-p}$ $(0 < p < m)$ and $D_m = 0$. The scheme is exactly time reversible [1]. Here, we consider an extended factorization scheme of the fourth-order by allowing one more stage than the minimum stage, i.e., five-stage integrators. We perform the similar approach as indicated in Ref. 4 based on the minimization of the truncation error-function to find the coefficients. The coefficients are finally given in Table 1. The norm of

TABLE 1 Coefficients of the Symplectic Integrators

	Two-stage second-order[4]	Five-stage Fourth-order[3]	Optimal five-stage Fourth-order
C_1	0.2928932188	0.17399689146541	0.1786178958
D_1	0.7071067810	0.62337932451322	0.7123418311
C_2	0.7071067810	−0.12038504121430	−0.0662645827
D_2	0.2928932188	−0.12337932451322	−0.2123418311
C_3	—	0.89277629949778	0.7752933737
D_3	—	D_2	D_2
CFL_{max}	0.56033	0.74394	0.72633

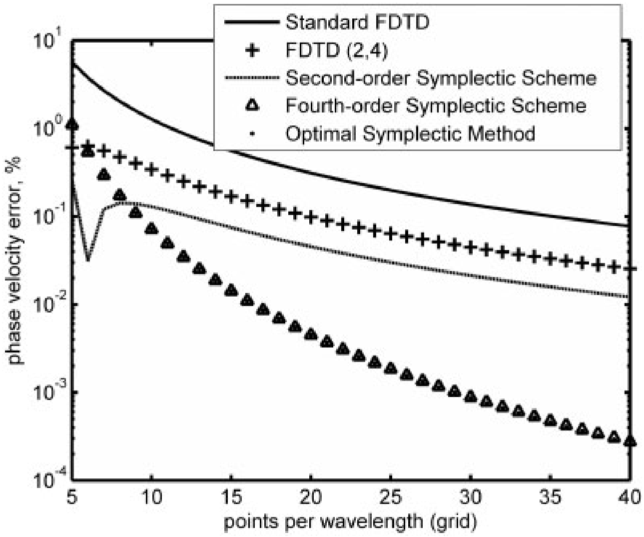

Figure 1 Dispersion curves for a plane wave traveling at $\theta = 0°$, $\phi = 45°$ with respect to the grid lines versus PPW discretization

the fifth-order error is 0.00061 in the optimal scheme when compared with 0.0069 of the scheme in Refs. 2 and 3. Thus, the optimal scheme is more accuracy.

2. STABILITY AND DISPERSION OF OPTIMAL SYMPLECTIC SCHEME

Maxwell's equations in an isotropic, lossless, and source-free medium can be written in a matrix form as

$$\frac{\partial}{\partial t}\begin{pmatrix} \boldsymbol{H} \\ \boldsymbol{E} \end{pmatrix} = (A + B)\begin{pmatrix} \boldsymbol{H} \\ \boldsymbol{E} \end{pmatrix} \tag{4}$$

$$A = \begin{pmatrix} \{0\}_{3\times 3} & -\mu^{-1}R \\ \{0\}_{3\times 3} & \{0\}_{3\times 3} \end{pmatrix},\ B = \begin{pmatrix} \{0\}_{3\times 3} & \{0\}_{3\times 3} \\ \varepsilon^{-1}R & \{0\}_{3\times 3} \end{pmatrix} \tag{5}$$

where μ and ε is the permeability and permittivity, $\{0\}_{3\times 3}$ is the 3×3 null matrix, R is the 3×3 matrix representing the curl operator. As indicated in Refs. 2 and 3, we use optimal symplectic integrators to discretizate Maxwell's equations in the time direction and then use a fourth-order accuracy to discretizate R in the space direction.

For the scheme to be stable, $|\varsigma| \leq 1$. The ς can be written as

$$\varsigma = 1 + \left(\frac{1}{2}\right)\sum_{p=1}^{5} g_p\left\{\frac{1}{\mu\varepsilon}\Delta t^2(\eta_x^2 + \eta_y^2 + \eta_z^2)\right\}^p \tag{6}$$

$$g_p = \sum_{l\leq i_1\leq j_1<i_2\leq j_2<\cdots<i_p\leq j_p\leq 5} C_{i_1}D_{j_1}C_{i_2}D_{j_2}\cdots C_{i_p}D_{j_p} + \sum_{l\leq i_1<j_1\leq i_2<j_2\leq\cdots\leq i_p<j_p\leq 5} D_{i_1}C_{j_1}D_{i_2}C_{j_2}\cdots D_{i_p}C_{j_p} \tag{7}$$

$$\eta_x = \frac{27(e^{-jk_x\Delta x/2} - e^{jk_x\Delta x/2}) - (e^{-3jk_x\Delta x/2} - e^{3jk_x\Delta x/2})}{24\Delta x} \tag{8}$$

$$\eta_y = \frac{27(e^{-jk_y\Delta y/2} - e^{jk_y\Delta y/2}) - (e^{-3jk_y\Delta y/2} - e^{3jk_y\Delta y/2})}{24\Delta y} \tag{9}$$

$$\eta_z = \frac{27(e^{-jk_z\Delta z/2} - e^{jk_z\Delta z/2}) - (e^{-3jk_z\Delta z/2} - e^{3jk_z\Delta z/2})}{24\Delta z} \tag{10}$$

$$k_x = k \sin\theta \cos\phi \tag{11}$$

$$k_y = k \sin\theta \sin\phi \tag{12}$$

$$k_z = k \cos\theta \tag{13}$$

where k is the wave number, ϕ and θ are the wave propagating angles with respect to x- and z-axis, respectively. In our numerical simulations, we use space discretizatations grid $\Delta x = \Delta y = \Delta z = \Delta$ and defined

$$\mathrm{CFL} = \frac{\Delta t}{\Delta\sqrt{\varepsilon u}} \tag{14}$$

The stability of the scheme is determined by the maximum of CFL, i.e., $\mathrm{CFL}_{\max}$. The numerical results for $\mathrm{CFL}_{\max}$ are also shown in Table 1. The optimal fourth-order scheme has almost the same $\mathrm{CFL}_{\max}$ as the scheme in Ref. 3, but larger than the second-order method in Ref. 4. The numerical dispersion can be expressed as

$$\cos(\omega\Delta t) = \varsigma \tag{15}$$

where ω is the radian frequency. Figure 1 shows the relative phase velocity error as a function of the points per wavelength (PPW) for a plane wave traveling at angle $\theta = 0°$, $\phi = 45°$.

Figure 2 shows the relative phase velocity error as a function of the propagating angle θ at $\phi = 0°$.

Figure 3 shows the relative phase velocity error as a function of the propagating angle ϕ at $\theta = 0°$.

For comparison with our optimal scheme, we also plot a two-stage second-order symplectic scheme [4], a five-stage fourth-order symplectic scheme [2, 3], standard finite-difference time-domain (FDTD) and a fourth-order spatial-difference FDTD scheme (FDTD (2, 4)) [5]. In all following simulations, we use CFL = 0.5. We can see from the figures both fourth-order symplectic integrators schemes acquire the same dispersion, and have less dispersion than the second-order symplectic integrators

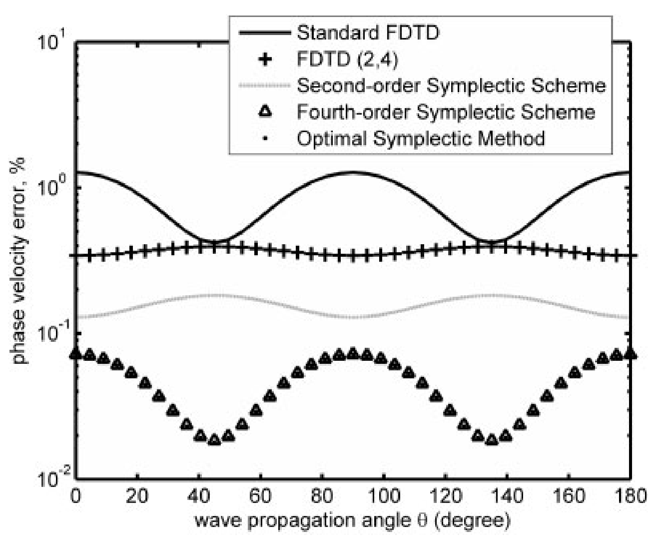

Figure 2 Dispersion curves for a plane wave traveling at $\phi = 0°$ with respect to the grid lines versus different angle θ at PPW = 10

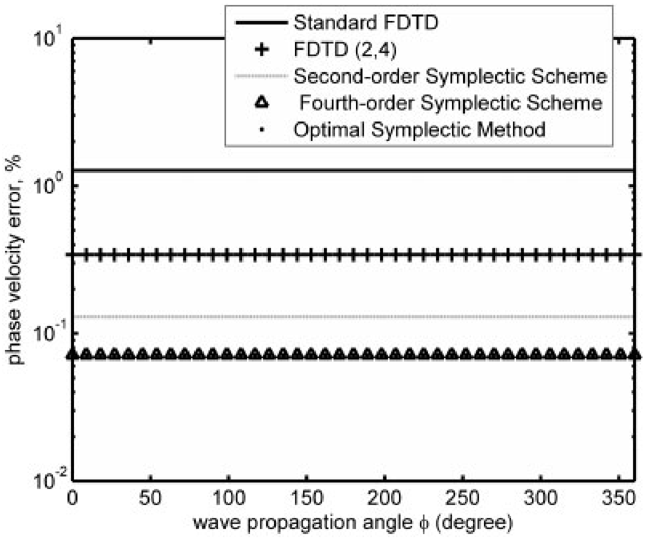

Figure 3 Dispersion curves for a plane wave traveling at $\theta = 0°$ with respect to the grid lines versus different angle ϕ at PPW = 10

scheme, standard FDTD, and FDTD (2, 4). Also, both fourth-order schemes permit a coarser discretization than other schemes for a given error bound, which, in turn, allow faster computation time and the storage of less data.

3. CONCLUSION

The proposed symplectic scheme is more efficient in the calculations at the same computational cost than the mostly used fourth-order symplectic scheme in Refs. 2 and 3, and provides a new approach for solving large computational domain electrodynamics problems.

ACKNOWLEDGMENT

This work was partially supported by "The National Natural Science Foundation of China (No. 60371041 and 60671051), China".

REFERENCES

1. J.M. Sanz-Serna and M.P. Calvo, Numerical hamiltonian problems, Chapman & Hall, London, U.K, 1994.
2. S. Wei, Z.X. Huang, X.L. Wu, and M.S. Chen, Total field and scattered field technique for fourth-order symplectic finite difference time domain method, Chin Phy Lett 23 (2006), 103–105.
3. T. Hirono, W. Lui, S. Seki, and Y. Yoshikuni, A three-dimensional fourth-order finite-difference time-domain scheme using a symplectic integrator propagator, IEEE Trans Mircowave Theory Tech 49 (2001), 1640–1648.
4. T. Kostas and T.E. Simos, Symplectic methods for the numerical solution of the radial Shrödinger equation, J Chem Phys 34 (2002), 83–93.
5. A. Taflove and S.C. Hagness, Computational electrodynamics: The finite-difference time-domain method, Artech House, Boston, 2000.

SIMULTANEOUSLY ALL-OPTICAL INVERTED AND NONINVERTED WAVELENGTH CONVERSION EMPLOYING SOA-BASED SAGNAC INTERFEROMETER

Zhixin Chen, Jian Wu, Kun Xu, and Jintong Lin
The Key Laboratory of Optical Communication and Lightwave Technologies of MOE, Beijing University of Posts and Telecommunications, Beijing 100876, People's Republic of China

Received 30 July 2006

ABSTRACT: *This paper have successfully demonstrated an all-optical wavelength conversion scheme for all-speed return-to-zero (RZ) format data at 10 Gbit/s rate by using a Sagnac interferometer based on semiconductor optical amplifier (SOA). The attractive issue of the proposed method is that the converted signal can be obtained simultaneously with inverted and noninverted wavelength conversion signals.* © 2007 Wiley Periodicals, Inc. Microwave Opt Technol Lett 49: 547–551, 2007; Published online in Wiley InterScience (www.interscience.wiley.com). DOI 10.1002/mop.22192

Key words: *all-optical wavelength converter; semiconductor optical amplifier (SOA); cross gain modulation (XGM); cross phase modulation (XPM); all-optical signal processing*

1. INTRODUCTION

All-optical wavelength converters are expected to become the one of key components in future optical networks. SOA-Based wavelength converters are becoming attractive because of their small size, cascadibility, and ease of integration. Meanwhile, based on the nonlinearities of SOAs, various simultaneously with inverted and noninverted wavelength conversions have been demonstrated. Schemes based on cross gain modulation (XGM) by use of two cascaded SOAs are fit for higher-speed operation but usually employ more than one SOA [1]. Schemes based on cross polarization modulation (XPloM) usually depend on accurate polarization control and power control, which is quite impractical [2]. Schemes based on cross phase modulation (XPM) by use of Mach-zehnder interferometer (MZI) also need two SOAs operation [3]. And to the best knowledge of the authors, schemes based on XPM by use of Sagnac interferometers are only achieved noninverted wavelength conversion of optical RZ signals [4] and inverted wavelength conversion of optical nonreturn-to-zero (NRZ) signals [5], Simultaneously all-optical inverted and noninverted wavelength conversion using SOA-based Sagnac interferometer has not been reported before.

Owing to the low pulse energy, high operating speed, compactness and in principle polarization independent, SOA-based Sagnac interferometers are the one of promising candidates for all-optical signal processing. Such as all-optical demultiplexing, optical computing, switching, regenerating, etc. In this letter, the paper is first time achieved simultaneously multifunction wavelength conversion using SOA-based Sagnac interferometer at 10 Gbit/s. Thus, this scheme may be useful in practical RZ-based high-speed wavelength-division-multiplexing (WDM) communication networks.

2. PRICINPLE OF OPERATION

Figure 1 shows the schematic diagram of simultaneously all-optical inverted and noninverted wavelength conversion based on SOA-based Sagnac interferometer, its principle is similar with [6, 7]. There are four ports, A, B, C, and D, and the whole loop is connected with the two couplers. Meanwhile, a SOA is placed at